Experimental report

01/06/2019

Proposal: **1-02-227** **Council:** 4/2017

Title: Stress Distribution and Strain Mapping in Porous Granular Rocks (II)

Research area: Engineering

This proposal is a new proposal

Main proposer: **Stefanos ATHANASOPOULOS**

Experimental team: Stephen HALL
Stefanos ATHANASOPOULOS

Local contacts: Thilo PIRLING

Samples: Cemented Quartz

Instrument	Requested days	Allocated days	From	To
SALSA	9	9	02/06/2018	11/06/2018

Abstract:

The mechanical behaviour of porous granular rocks is highly complex due to the fact that they exhibit a multiscale interaction of three different phases: grains, cement and pores. Recent experiments at ISIS (ENGIN-X), as well as an ongoing experiment on SALSA, have proven that neutron diffraction scanning during in-situ loading tests can aid in the understanding of the (micro-)mechanisms that act during the deformation and eventually lead to failure of such materials. In the proposed experiment, which is a continuation of experiment 1-02-165 (no report submitted since it is ongoing at the time of writing), a new version of a plane-strain loading device will be used towards the complete assessment of the deformation mechanisms of granular materials than has previously been possible. More specifically, the new device will allow the neutron diffraction strain scanning measurements of the elastic crystallographic (grain) strains to be compared to the total strains, which will be acquired by the simultaneous use of Digital Image Correlation.

This report concerns the experiment 1-02-227 carried out on SALSA. The aim of the experiment was to to use Neutron Strain Scanning (NSS) to produce full-field mappings of the granular-strain and, therefore, stress distribution in a sand specimen under load, whilst simultaneously acquiring photographs of the specimen through a sapphire glass window, to produce (through Digital Image Correlation – DIC) the total strain field throughout the material.

The experiment involved a prismatic specimen (height 60 mm, width 30 mm, thickness 20 mm) of Fontainbleau NE 34 quartz sand (average grain size: 210 µm) loaded in a specially designed plane-strain apparatus (Fig.1). The plane-strain conditions with this apparatus are fulfilled by applying a force along the longitudinal axis of the specimen (in this case, with the in-situ SALSA stress rig mounted on the hexapod) and deformation being limited to develop in only one of the other two directions, through the combination of a pair of deformable, pressure-controlled cushions and a pair of sapphire platens, which prevent any deformation in the third direction.

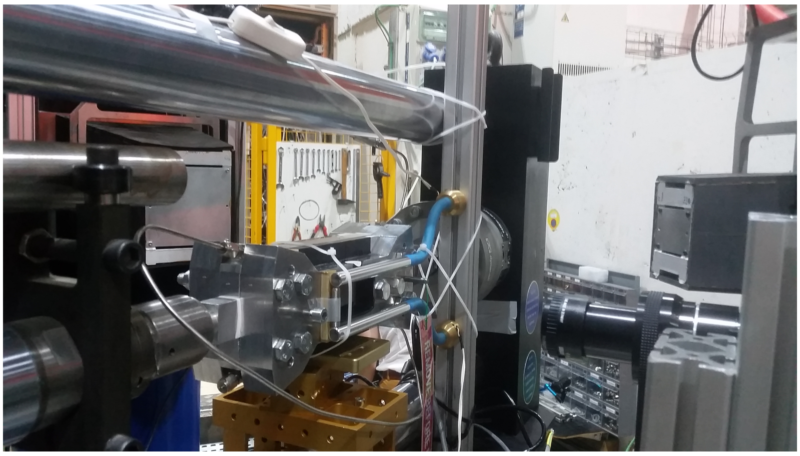

Figure 1: The experimental setup in the SALSA neutron strain scanner.

The loading of the specimen was realised over a load-unload cycle (Fig.2). The first stage of the loading involved attaining a confining pressure of 2 MPa (applied with a user-provided water pump through the pressure-controlled cushions) with simultaneous increase of the axial stress, to maintain in-plane pressure boundary conditions. Subsequently, the specimen was loaded over a series of load steps, reaching a maximum axial stress of approximately 15 MPa. At each load step, the loading was paused, with the axial displacement and confining pressure held constant, to acquire diffraction data over a 2D grid of 78 points in the middle of the specimen. The scanning coverage of the specimen was approximately 75% (of the initial dimensions of the specimen), using a 4x4x4 mm^3 gauge volume (GV) and the count time for each GV was 3 min. In parallel, photographs for the DIC were acquired every 3 min during the NSS measurements and every 5 s during the loading of the specimen.

Figure 2 shows the DIC-derived axial component of the total strain field, $\varepsilon_{\mathrm{DIC,axial}}$, and the NSS-inferred total $\sigma^{211}_{\mathrm{axial}}$ mappings (Fig.2(b)) for selected load steps, together with the macroscopic axial strain as a function of the applied axial stress (Fig.2(a)). In the initial, deviatoric part of the loading (i.e., after the isotropic loading of 2 MPa had been attained) and up to approximately 9 MPa, the macro-curve is almost linear (i.e, the material is in the elastic region of the loading), showing only a slight change in its gradient. From that point on and until the yielding point is reached, the gradient gradually decreases with respect to time, eventually becoming nearly flat (i.e., there is no clear yielding point reached). In theory, the yielding point of the material should had been clearer and further to that, the attained maximum load was expected to be less. This can be associated with the highly discontinuous (due to the large number of load steps) and slow (due to the long pauses for the NSS measurements to take place) loading of the material, which most likely allowed a more smooth rearrangement of the sand grains throughout the loading (i.e., during the pauses the stress rig was set in displacement control and thus, the specimen was into a relaxation mode). By extension, the – theoretical – development of the localisation of deformation (into one or more shear bands leading ultimately to the failure of the specimen) at the pre-yielding stages, is expected to also have been affected by this smooth rearrangement of the grains. Eventually, the material exhibits complete yielding and gradually enters a post-yielding plateau that can be correlated to the evolution of the formed shear band(s) and significant grain crashing.

The 2D diffraction mappings at each load step show the evolution of the spatially resolved micro-stress distribution. In the mappings of the first load steps (i.e., load steps 4 to 6) significant variations are exhibited (i.e., areas that appear to be more stressed at some load level shift to a lower stress state at a subsequent load level, whereas neighbouring areas exhibit the opposite behaviour, and vice versa). These shifts likely indicate grain re-organisation and porosity reduction. With the increase of the applied load (i.e., approximately at 9 MPa – load step 12) large areas of the mappings become darker (i.e., more compressed), but the variations do not seem to come to an end (i.e., load steps 12 to 15). These – varying – large areas seem to have an inclined structure, indicating that diagonal features start becoming more pronounced. The diagonal features, extending from the top left and right corner of the mappings to the middle of the right and left hand-side, respectively, may be interpreted as principal localised deformation bands (i.e., shear bands) in an early stage. The fact that variations still exist at even higher load levels (i.e., load steps 19, 20 and 23) possibly means that the localised deformation mechanisms, within and in the vicinity of the regions where these main diagonal features extend, continue to develop. These results seem to be consistent with the assumption that the localised deformation was affected by the discontinuous and slow loading of the specimen that – most likely – resulted in a smooth rearrangement of the grains between load steps. The final mappings (i.e., load steps 25 and 26) exhibit – to a certain extent – an opposite structure (i.e, the former has a prevailing diagonal structure extending from the top left corner of the mapping to the middle of the right hand-side, whilst the latter, the opposite). Further to that, the mapping acquired immediately after the yielding point (i.e., load step 25) appears to be less compressed compared to the mapping acquired during the post-yielding plateau. This suggests that with the slipping of a primary principal shear band (i.e., from top left to middle right), the stress becomes less localised, as it leads towards the activation (and eventually slipping) of another, secondary shear band (i.e., from top right to middle left).

Regarding the comparison of the NSS mappings to the DIC results, a relatively good and, in certain cases, prominent correlation can be made. Further investigation is needed to understand the features that do not correlate between the DIC and NSS results described above. Is is noted though, that since the two techniques measure different properties, complete structural agreement between the two should not be expected and these differences might reveal more information on the mechanics.

This, second experiment (first being experiment 1-02-165) on a sand specimen is considered successful, first of all due to the fact that both the spatial and the temporal resolution of the measurements have been increased significantly (i.e., 11% coverage and 11 mappings for the previous experiment, versus 75% coverage and 31 mappings for the current experiment). Further to that, even from the preliminary analysis of the results a considerable amount of information has been revealed regarding the (micro-)mechanisms of deformation in granular geomaterials, by associating measurements at multiple scales (i.e., the traditional macroscale measurements to the mesoscale characterisation of the strain field (through DIC) and the inferred microscale stress distribution (through NSS)). After the data have been fully processed (i.e., optimisation of the peak fittings and refinement of the produced NSS micro-stress mappings and DIC strain fields), they will provide novel insight towards the understanding of how forces are transmitted through granular material and how this leads eventually to failure.

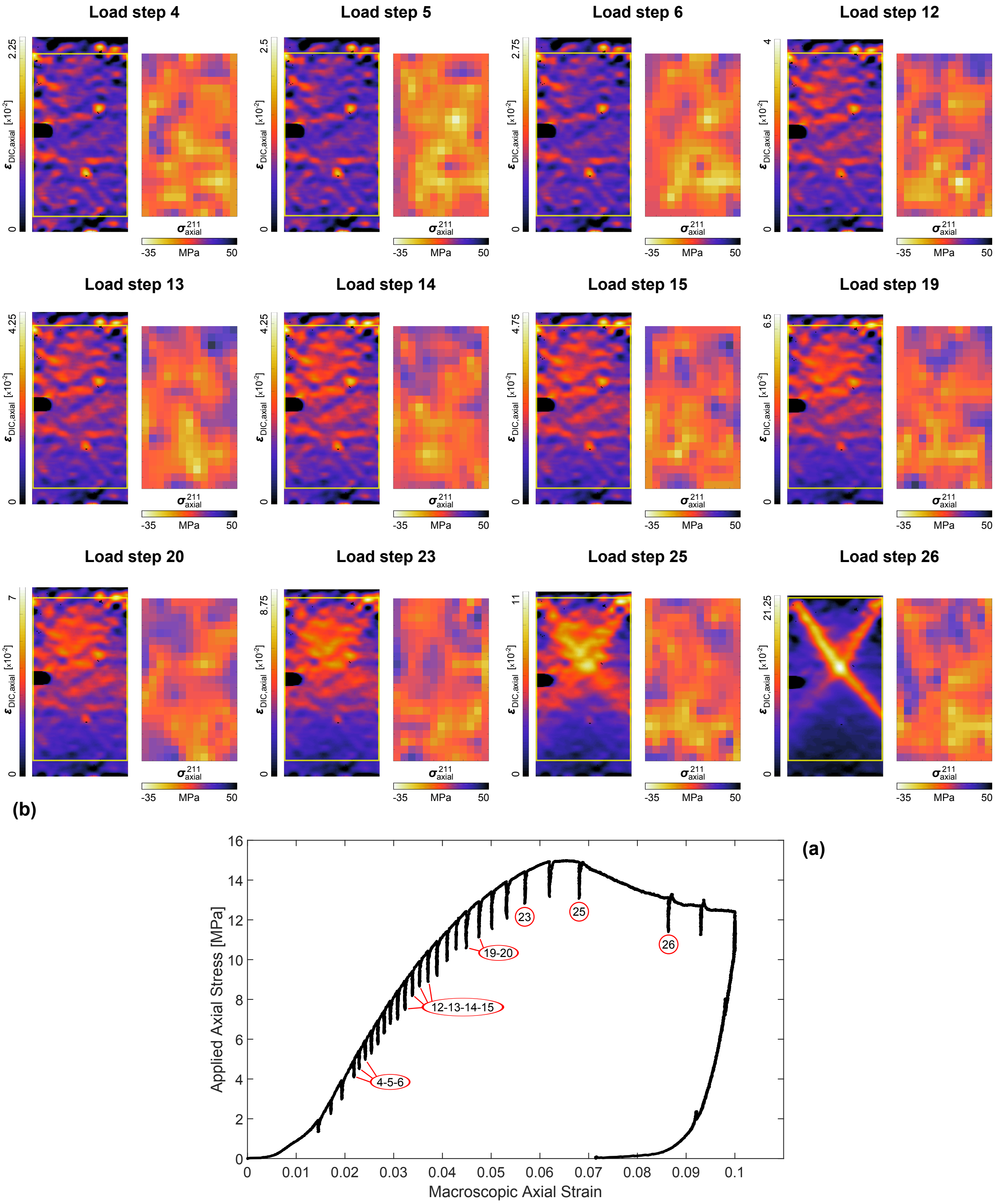

Figure 2: (a): The macroscopic axial strain as a function of the applied axial stress. (b): The DIC-derived axial component of the total strain field (left) and the NSS-derived mappings of the axial component of the total micro-stress (right) for selected load steps.